2018 IEEE/RSJ International Conference on Intelligent Robots and Systems (IROS)
Madrid, Spain, October 1-5, 2018

Maneuverability in Dynamic Vertical Climbing

Jason M. Brown, Max P. Austin, Bharat Kanwar, Tyler E. Jonas, and Jonathan E. Clark

***Abstract*— In this paper, we examine the reduced order pendular dynamic climbing model with the addition of attachment windows based on prescribed body roll. With this model and on the new dynamic climbing platform, TAILS, we demonstrate dynamic downward climbing as well as identify distinct dynamic gaits within downward climbing. This, combined with the application of an asymmetric configuration of the rear legs enables strafing motions and thus dynamic maneuverability on walls in the vertical domain.**

I. Introduction

While slow, or quasi-static, maneuverability (both in the horizontal and vertical domain) is relatively well understood and achievable through kinematic control [1]–[3], dynamic maneuverability for high speed dynamic runners and climbers is most effective when forces redirect the momentum of the system. Reduced order dynamic models, such as 3D SLIP and LLS have shown that rapid turns can be achieved by inducing a small touchdown position offset [4], [5]. By applying the understanding from the above models to running robots such as iSprawl, Rhex and Minitaur, dynamic maneuverability has been achieved using small servos or phasing offsets of legs to generate the forces necessary for rapid turns [6]–[8]

While reduced order dynamic models of turning exist in the horizontal domain, reduced order modeling of climbing, which has been shown to be captured by the Full-Goldman (FG) template, has been primarily restricted to vertical motion [9]. Unlike comparable examples in the horizontal domain, the dynamics of the FG template are designed to run directly against gravity, limiting the range of achievable heading angles.

Recently, climbing robots based on this model, such as DynoClimber and BOB have been able to achieve vertical speeds of 65 cm/s [10] and 1.95 body lengths per second [11] respectively. While some strafing motions have been achieved in the upward direction [12], to achieve dynamic maneuverability, downward gaits along with downward strafing are required.

In this paper we examine an extension of the pendular dynamic climbing model which begins to incorporate out of plane dynamics and study how these can be utilized to generate dynamic maneuverability with upward locomotion and, for the first time, generate dynamic downward climbing. These insights are applied to a new dynamic climbing platform TAILS, shown in Fig. 1a, which can independently control nominal body pitch and roll.

FAMU/FSU College of Engineering, Tallahassee, FL 32310 email: jmb10t@my.fsu.edu

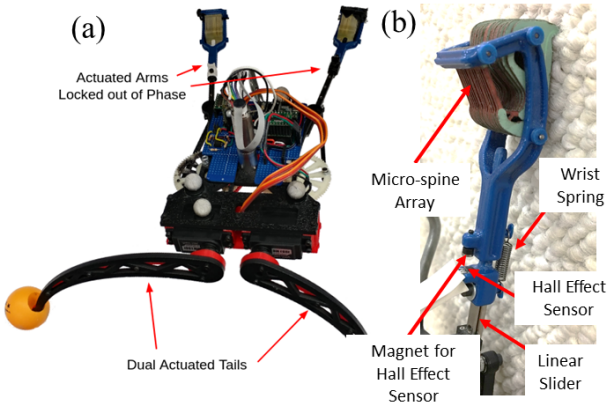

Fig. 1: a) TAILS robot with phase locked front limbs and independently actuated rear limbs which enable decoupled pitch and roll control. b) Microspine array from front limbs which enables attachment onto surfaces such as stone and cinder block and incorporates the Hall-effect based force sensor.

II. Models

A. Full Goldman Model

The purely transverse plane Full-Goldman template, which consists of 2 springy prismatic arms at a fixed lateral and angular offset from the center of mass (COM) and a distributed body mass, has been shown to capture the total ground reaction forces and COM motions of both geckos and cockroaches [9]. The template assumes attachment to a surface occurs at maximum leg extension, with attachment behaving as a pin joint, while detachment is assumed to occur when the leg reaches max compression. Actuation of the nominal rest length is defined by a sinusoidal length trajectory.

The dynamic climbing model, shown in Fig. 2a, is a reduced order model to the Full-Goldman template and reduces the distributed mass to a point mass thereby ignoring the moment of inertia. The 2 prismatically actuated springy legs are then defined from the COM with a fixed angular offset. While initial studies with this model [10] maintained the timing/actuation based attachment assumptions, more recent versions have incorporated directional adhesion where attachment occurs when the foot is moving down a surface and detachment occurs when the ground reaction force in an individual foot reaches zero.

The equations of motion for the dynamic climbing model used in this study have been previously derived in Brown et al. [13] and are defined to handle the cases where a

978-1-5386-8094-0/18/$31.00 ©2018 IEEE

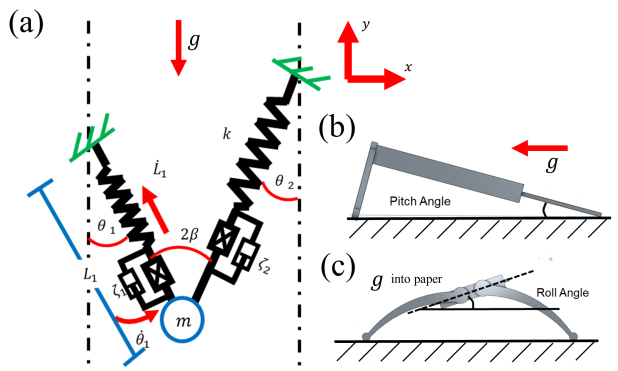

Fig. 2: a) The non-conservative Pendular Dynamic Climbing Model consisting of a point mass and 2 linearly actuated springy arms at a fixed angle offset. b) and c) Quasi-static 3D model of FG inspired climbers which defines attachment windows based on roll.

Parameter	Description	Value
g	Gravitational Constant	9.81 ms^{-2}
i	Leg Identifier	[0 or 1]
Leg_i	Flag for Attachment of Leg i	[0 or 1]
L_{nom}	Nominal Length of Leg	0.2 m
L_{stroke}	Stroke Length of Leg	0.05 m
k	Spring Stiffness of Leg Spring	250 Nm^{-1}
β	Sprawl Angle	20 deg
b	Damping	0.2 N s m^{-1}
m	Body Mass	0.3 kg
Ω	Driving Frequency	1-6 Hz
Φ	Phase Shift	0-100 % of the period
Θ_{off}	Amplitude Offset	-10-10 deg

TABLE I: Parameter settings for climbing sweeps.

single leg, both legs, and no legs attach to the surface. This flexibility in phases enabled the model to demonstrate and define distinct dynamic gaits within climbing, with dynamic walking, running, and high speed compliant running. The equations of motion are non-conservative, with linear viscous damping included along the prismatically actuated legs. In addition to this, TAILS constrains the legs to a sinusoidal leg extension, with the legs phase locked 180° out of phase.

B. Out of Plane Dynamics

In order to begin to explore the potential applications of out of plane motions as well as explore their potential interaction with dynamic climbing gaits, the attachment conditions defined for directional adhesion are refined here to account for induced body roll as seen in the quasi-static model, shown in Fig. 2b and c. This model represents the morphology of dynamic climber robots, consisting of 2 prismatic arms above the COM at a fixed offset at the centerline as well as 2 passive rear feet which were defined to be both behind and below the COM [11]. By prescribing an induced body roll with a sinusoidal trajectory, the attachment condition of directional adhesion (the foot beginning to move down the surface) is only applied if the specific foot is rolled toward the wall. Otherwise, the foot is free to fall down the surface. Foot velocity and body roll then combine to define attachment windows where attachment is capable of occurring for each leg.

The frequency of the sinusoidal roll trajectory is set to match the frequency of the sinusoidal prismatic actuation and a phasing parameter Φ is introduced which defines the timing offset between the start of the roll and prismatic actuation. In addition to this, the roll sinusoid can be set with a amplitude shift which changes the nominal angle of the roll and induces an asymmetry in the attachment windows.

III. Simulation

The dynamic climbing model described in sections II-A and II-B was set up to test the potential applications of the out of plane attachment constraints on the FG dynamics. Of special interest was if, by proper tuning of the attachment window, dynamic downward climbing and strafing behaviors emerge (which are prerequisites for dynamic maneuverability). Additionally we investigate if downward climbing has distinct gaits (i.e. walk, run) and if they are the same gaits as upward climbing.

A. Simulation Procedure

The parameters for the climbing model, shown in Table I, were set to match past experimental results of the BOB 2.0 robot [14], with the parameters of driving frequency, phase shift, and roll actuation amplitude offset being swept. Previous simulations have demonstrated the presence and location of transition points between dynamic walking, running, and compliant running by sweeping frequency from a value of 1Hz to 6Hz (the upper limit of BOB 2.0 [14]).

Sweeping the phase offset Φ from zero to 50% of the period changes the roll and prismatic actuation from being completely out of phase, which should impact the attachment window, to completely in phase with the leg actuation, which should not. The amplitude offset (from -10 to 10 deg) changes the nominal set point of the roll which modifies the attachment windows for the left and right legs asymmetrically. By enabling one leg to attach earlier in its steady state cycle, the effective stroke length of that leg should be lengthened compared with the other leg which should induce strafing [12].

Two distinct 2D parameter sweeps were performed, the first varying frequency (from 1-6 Hz at a resolution of 0.05 Hz) and phase shift (from 0-100 % of the period at a resolution of 1%). The second sweep varied driving frequency (from 1-6 Hz at a resolution of 0.05 Hz) and Roll Amplitude Offset (from -10-10 deg at a resolution of 0.2 deg). A Newton-Raphson fixed point search was implemented to determine steady state behavior at each parameter set, with the climbing velocity, measured as the average over the course of a stride, and the duty factor, measured as the fraction of the period one leg is in stance, recorded for each successful gait. For the roll amplitude sweep, the mean horizontal velocity over the course of a stride was recorded

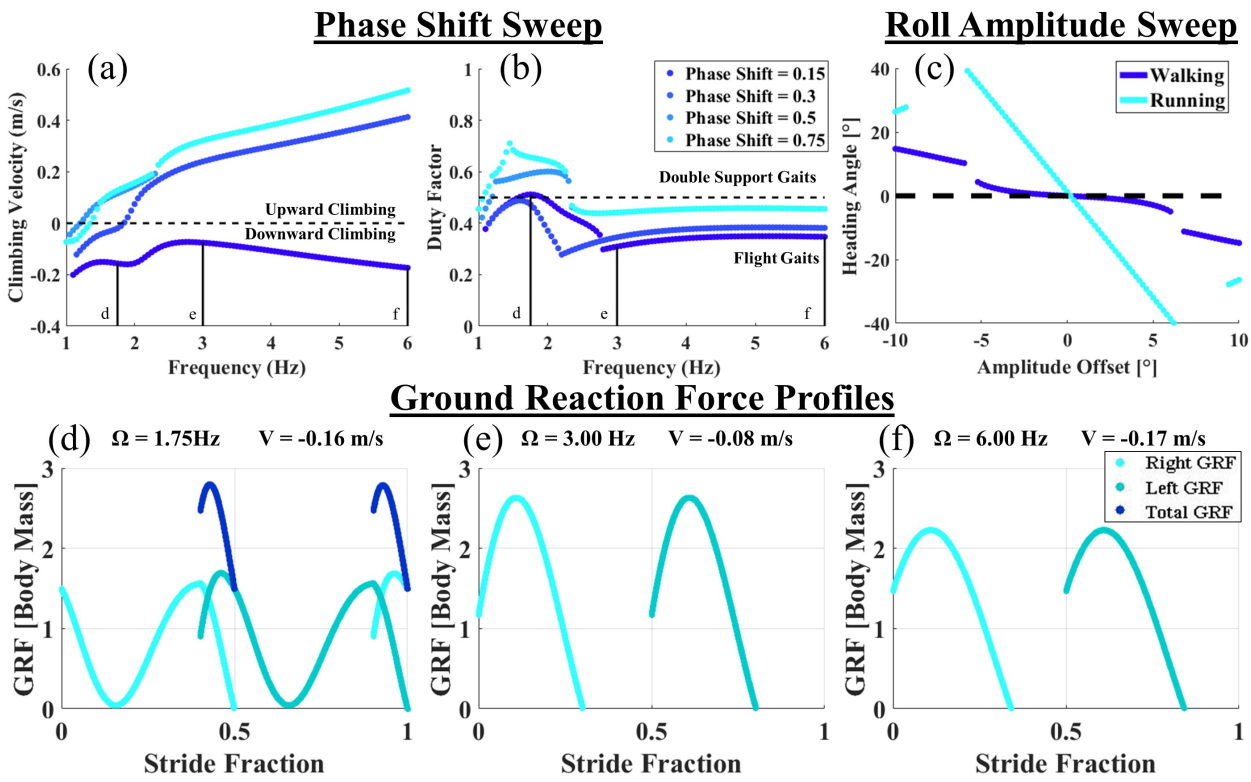

Fig. 3: a) and b) The climbing velocity and duty factor of 4 discrete phase shifts as frequency is swept. At a phase shift of 0.15, the entire frequency range is downward. The duty factor provides ranges of dynamic gaits, where for downward climbing, a gait transition occurs around 2.8 Hz. c) The effective heading angle as the roll amplitude offset is swept for the downward climbing gait, which shows that significant strafing only occurs for running gaits. d) e) and f) show the the ground reaction forces at 1.75 Hz, 3.00 Hz, and 6.00 Hz respectively. d) has the double peak profile representative of walking while e) and f) have the single peak profiles representative of running.

and transformed into heading angle with:

$$\arctan\left(\frac{V_{hor}}{|V_{vert}|}\right) \tag{1}$$

where V_{hor} is the mean horizontal velocity and V_{vert} is the mean vertical velocity.

B. Simulation Results

1) Impact of Phase Shift: Fig. 3(a,b) show the results from the 2D sweep of driving frequency versus phase shift. At low frequencies (below 1.5 Hz), virtually every phase shift resulted in downward climbing. While all of these gaits climbed downward, phase shift had a significant impact in the climbing velocity, with speed varying from -3.2 cm/s to -21.8 cm/s for a 1 Hz driving frequency.

Above these frequencies, the downward climbing was only found in a very narrow range of phase shift values of 0.13 - 0.18 of the period. In the phase shift region above these gaits (0.18 - 0.40), the velocity increases almost linearly with phase shift while remaining nearly constant with frequency. For phase shift values above this (0.40 to 1.00), the climbing velocity shows no correlation to phase shift and matched previous climbing velocity trends [14].

The duty factor of the downward climbing gaits exhibit a discrete transition just below 3 Hz, suggesting that there is a gait transition at this frequency. However, unlike upward climbing, where the initial gait had duty factors above 0.5 (meaning double support phases), downward climbing spans a range from 0.4-0.55, meaning both flight phases and double support phases are present in the lowest frequency gait.

One metric applied to identify gaits during upward climbing is the ground reaction force profiles, where double peak ground reaction forces suggested a walking gait while single peak profiles suggested running gaits. Examining the ground reaction force profiles of the downward climbing gait at 1.75 Hz, shown in Fig. 3d, the profile exhibits a double peak ground reaction force characteristic of walking The moderate frequency gait at 3 Hz, shown in Fig. 3e, which is shortly after the potential gait transition identified from the duty factor change, there is single peak ground reaction force profile and a significant aerial phase. Finally at the highest frequencies tested, shown in Fig. 3f, the ground reaction force profile still has a single peak but the peak is slightly lower than the moderate frequencies. It, however, does not exhibit the previously seen compliant running behavior with a double support phase. Together these results reveal the presence

of two distinct gaits for downward climbing, walking at frequencies below 3 Hz and running above that transition point.

2) Impact of Amplitude Offset: The results from the amplitude offset sweep, shown in Fig. 3c, which was conducted for purely downward climbing gaits (since upward strafing has been previously demonstrated by Dickson et al. [12]) shows that as frequency is increased, the horizontal velocity also increases. For the lowest frequency gaits, this horizontal velocity is small, but higher frequency gaits have horizontal velocities close to the vertical velocities, indicating significant strafing.

IV. Robot Design

A. Platform Design

An improved version of the dynamic climber BOB 2.0 shown in Fig. 1c, named TAILS, was developed to implement body orientation control. The base dynamics of BOB were maintained by using the single drive motor for the phase locked front limb actuation, the outwardly sprawled forelimbs, and front feet which utilize micro-spine arrays [15] (which are capable of attaching to surfaces such as stone aggregate and cinder block), hall effect based force sensors on each wrist, and an indexing sensor to ensure timing sync between prismatic and roll actuation. The micro-spine arrays combined with the force sensors are shown in Fig. 1b. and are specifically designed to enable moderate strain, non-invasive force sensing at each wrist, which allows the capture of experimental ground reaction force profiles.

TAILS differs from previous FG based climbers by implementing independently actuated rear feet, which enables independent control of the body pitch and body roll (assuming both rear feet are in contact with the wall). The end effectors on the rear feet were initially 3D printed spheres. These resulted in significant drag when attempting to climbing both upward and downward, so larger, low friction spheres were placed around the original feet.

B. Controller Design

Based on the simulation data, defining the roll, θ, with a sinusoidal trajectory should enable downward climbing. For the physical implementation, however, the prescribed roll profile on TAILS also varies the actuation speed and thus energy in the out-of-plane direction. This can be regulated by including an additional parameter, hold duration (T_{hold}), with the resulting trajectory shown in Fig. 4. By setting this parameter to 0% of the period results in a pure sinusoid, the other extreme of 50% of the period results in a purely discrete/step roll trajectory. Additionally, unlike simulation, past experimental work with FG climbers required a sufficient pitch angle ϕ of the body in order to consistently attach to the wall.

With the added actuation capability at the rear feet, a controller was required to define the desired leg angles $\psi_{0,1}$. To start with, the forward kinematics defining the current pitch and roll are defined, and these equations are then

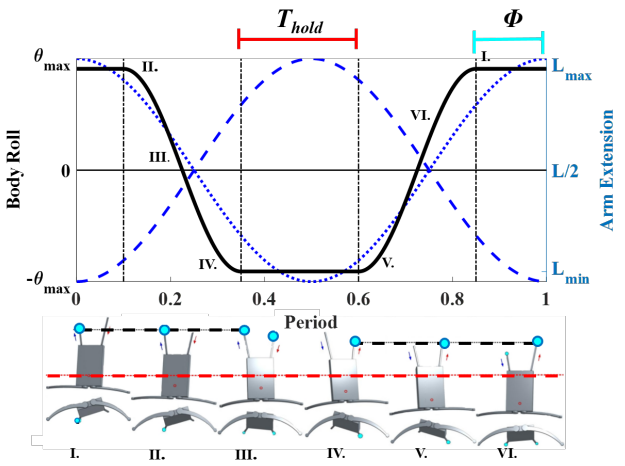

Fig. 4: Top) shows a representative body roll function which is shifted from the leg actuation by the phase shift Φ. The parameter T_{hold} modifies the roll function between a sinusoid to a square wave, which modulates the roll actuation speed. Bottom) the attachment conditions of the quasi-static model based on the prescribed roll function, with the various points in the trajectory labeled I-VI.

inverted to produce relations for the leg angles based on the desired roll and pitch.

1) Pitch: From the previous quasi-static modeling [11], the current pitch of the body ϕ is defined by the vertical offset of the rear leg L_{height} and the length of the body L_{body} (which is the sum of the torso length L_{torso} and the average leg length L_{nom}) using the following equation:

$$\phi = \arcsin\left(\frac{L_{height}}{L_{body}}\right). \tag{2}$$

2) Roll: Roll θ can be defined from the center axis based on the vertical distance from the centerline to the contact points with the wall, which is determined by the length of the rear leg L_{rear}. With TAILS, the axes of rotation for the legs servos are offset from the centerline by a distance L_{off}. Thus the body roll θ is defined by equation:

$$\theta = \frac{L_{rear}(\sin(\psi_0) - \sin(\psi_1))}{L_{off}} \tag{3}$$

3) Leg Equations: By inverting Eq. 2 and 3, the desired leg angles for a given roll and pitch can then be defined by:

$$\psi_i = (1-2i) * \sin^{-1}\left(\frac{L_{body}}{L_{rear}}\tan(\phi) + \frac{L_{off}}{2L_{rear}}\sin(\theta)\right) - \theta \tag{4}$$

where i represents the desired rear leg and has a value of either 0 or 1.

V. Experimental Procedure and Results

A. Experimental Design

For each trial, the COM position and orientation was recorded using a 6 Vicon Motion Tracking cameras at 300 Hz, with power provided by an off board power supply set to 15 V to reduce variation from battery drain, and a

Parameter	Value Range	Units
Driving Frequency	1, 1.5, 3	hz
Phase shift (Φ)	0,15,30,50,65,80	%
T_{hold}	0, 15, 50	%
Pitch (ϕ)	15, 25	deg
Roll Magnitude (θ_{max})	10, 25	deg

TABLE II: Parameters used in parameter sweep.

safety tether was held slack over the robot in case of a fall. A carpeted wall was used as the climbing substrate as its regularity makes it easy to attach to with the mircospine arrays. While the predicted trends of the simulation were tested via a parameter sweep, the optimal performance was determined using a Nelder-Mead optimization.

1) Parameter Sweep: The five parameters chosen for the experimental sweep, shown in Table II, are driving frequency of the prismatic actuator, the phase shift between the prismatic and roll actuation, T_{hold} which adjusts roll actuation from a sinusoid to a square wave, the magnitude of the roll actuation, and the nominal body pitch. The driving frequencies were selected to span a range of gait behaviors (walking to running), with the discrete values chosen based on preliminary testing results. The extreme values of T_{hold} were selected to span the maximum variation in roll energy addition, with an intermediate value selected based on initial hand tuned gaits. The values for the roll magnitude and body pitch were set near the extremes of achievable behavior. Finally, a range of the phase shifts, which in simulation resulted in downward climbing, was set to capture as many critical points as possible.

At the highest and lowest frequencies, the phase shift range was reduced in order to reduce the total number of trials. The highest frequency was only swept within the upward climbing region, phase shifts from $50-80\%$, as simulation and preliminary testing did not show any downward climbing in this region. The lowest frequency was only swept within the expected downward climbing range, phase shifts from $0-50\%$, as no previous experimentation with BOB and BOB 2.0 or simulation produced upward climbing gaits at this frequency.

2) Optimization: In order to fine tune performance, an optimization for downward climbing was performed. The drive frequency was held constant at 1 and 1.5 Hz and the remaining four control parameters were optimized using the direct search Nelder-Mead optimization which has been previously implemented to experimentally tune robots [16], [17]. The initial simplex used parameter sets from the parameter sweep that achieved downward climbing. Both phase shift and hold duration had access to their full range within the bounds: $0-100\%$ and $0-50\%$ respectively. The pitch and roll magnitude had ranges from 5° above their highest angle and below their lowest angle used in the parameter sweep.

The cost function for the downward climbing optimization was designed to find fast and stable downward climbing, with stability/consistency of the gait being weighted very highly. The cost function used consistency of the gait (measured via the standard deviation of the stroke length) to increase the stability and repeatability of a gait. Since fast behavior was also desired, the denominator of the cost function was set to the absolute value of the average climbing velocity. The weights for these parameters were hand tuned to match the relative magnitudes of the velocity and standard deviation. During experimentation, the robot was occasionally assisted with the supporting tether solely to move the robot past the transient phase and allow gaits which are sensitive to initial conditions the opportunity to succeed.

$$cost = \frac{1+1000*Std_{stroke}}{10*|V_{avg}|} \tag{5}$$

3) Strafing: In order to induce strafing, experiments were run using a fixed angular offset of the robot's tail. It was chosen not to actuate the rear feet as these experiments were primarily upward and the attachment windows for upward climbing can be achieved purely through the natural corrective orientation dynamics induced by the feet. A coarse parameter sweep of frequency and offset angle was used to find the ranges in which strafing manifested. Driving frequencies of $2Hz$, $3Hz$, and $4Hz$ were used and roll angles were set to be $\pm5^\circ$, $\pm10^\circ$, and $\pm15^\circ$. A constant pitch of 19° was used, the same as the nominal pitch of BOB.

B. Results

1) Parameter Sweep Results: The parameter sweep resulted in small regions of successful downward climbing gaits in about 10% of the gaits with phase shifts between 0 and 50% at frequencies of 1 Hz and 1.5 Hz. Examining the out of plane energy (approximated by the square of the angular velocity), in the roll direction, shown in Fig. 5(top), shows the downward gaits have significantly more roll energy than comparable upward climbing gaits. The difference in energy is most significant at the transition between upward climbing at 1.5 Hz, where the nominal roll energy of the downward gaits was 10 times higher than the upward climbing gait. The yaw energy Fig. 5(bottom) does not show as significant a correlation to climbing velocity, but does have a significant downward trend with frequency, suggesting that as the robot moves faster, these in-plane swing dynamics become less relevant.

While all successful downward gaits required the maximum roll magnitude of 25°, the other parameters showed less correlation as gaits were able to succeed at both pitches, hold durations of 0 and 15%, and phase shifts between $15-50\%$ for 1 Hz and $15-65\%$ at 1.5 Hz of the stride period. The upward gaits were generally successful, with failures at 3 Hz occurring at parameters which generated more roll energy than successful gaits.

2) Optimization Results: Table III shows the resulting parameters to which the optimization converged. At the lower frequency the gaits converged to high pitch and roll values and low phase shifts and hold durations. During testing it was seen that only gaits with high roll values were successful in climbing down, as seen in the parameter sweep. Although some gaits were seen to work with higher hold durations

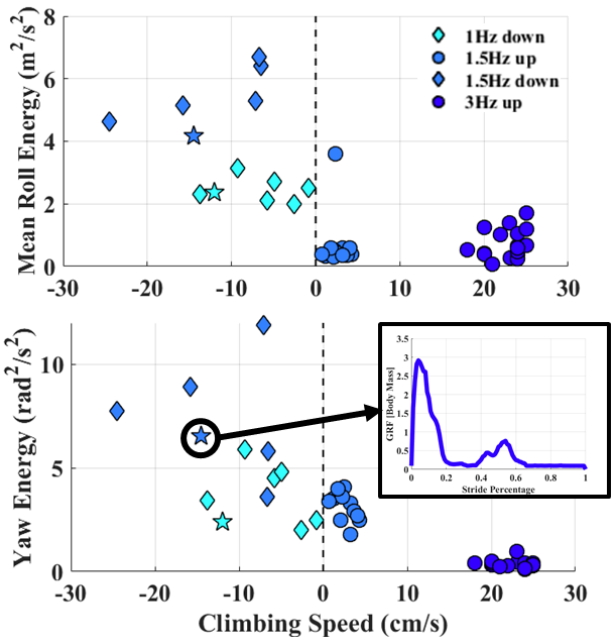

Fig. 5: (Top) The experimental mean roll energy of successful gaits from the parameter sweep and the optimal point (shown as the star) verse the climbing velocity. The downward gaits have significantly more mean roll energy. (Bottom) The mean yaw energy verse climbing velocity decreases significantly for upward running. (Inset) the experimental ground reaction force profile of the optimal point of the 1.5 Hz climbing gait.

Parameter	Value		Unit
Frequency	1.0	1.5	Hz
Phase shift	6.13	17.31	% of stride period
T_{hold}	0	6.22	% of stride period
Pitch	24.82	17.51	deg
Roll Magnitude	25.31	22.65	deg
Cost	2.089	2.157	
Downward Velocity	12.4	12.5	cm/s

TABLE III: Optimum Parameters

and lower pitches these tended to be less stable and resulted in higher deviations in stroke length. Phase shifts which were successful ranged from $5-17\%$, thus no gaits were successful at zero phase, identical to the parameter sweep.

The higher frequency optima converged to similarly high roll magnitudes however both the phase shift and hold duration are higher with the pitch value lower. These gaits generally resulted in climbing with visibly higher out of plane energetics. Failures occurred more frequently with smaller variance in parameter sets, but spanned a larger range suggesting parameter coupling effects are more significant at the higher frequency.

The experimental ground reaction force of the optimal 1.5 Hz downward climbing gait, seen in the subfigure in Fig. 5, has a double peak ground reaction force profile characteristic of walking gaits. This matches our simulation results for this frequency, which suggests that the dynamic

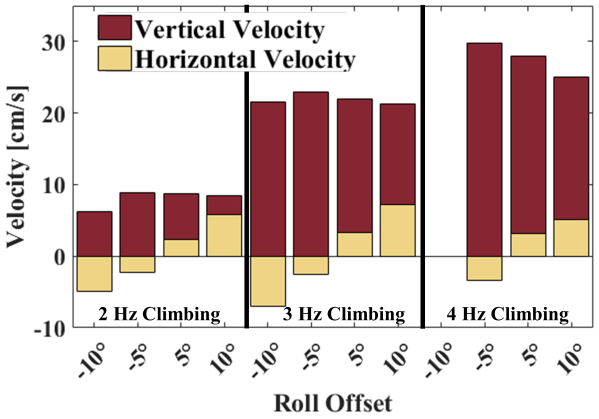

Fig. 6: The vertical (garnet) and horizontal (gold) velocities as frequency and amplitude offset are varied. Across driving frequencies, the horizontal velocities remain relatively constant while the vertical velocity increases significantly

climbing achieved was limited to dynamic walking gaits.

3) Strafing Results: Fig. 6 shows the resulting upward and lateral velocity of the strafing experiments. The figure shows that at fixed roll angles the lateral velocity has only slight variance over a range of frequencies. Upward velocity, on the other hand, shows very little sensitivity to the magnitude of the roll offset regardless of climbing frequency. The robot was able to succeed at roll values less than 10° for most frequencies and was unable to succeed at magnitudes of 15° or greater. The robot did experience a failure at the highest frequency when rolled -10°. This was likely due to slight asymmetry in the robot, or attachment in the testing environment.

VI. Discussion

A. Dynamic Climbing Maneuverability

While this paper explicitly considered inducing body roll to achieve dynamic maneuverability with TAILS (see Fig. 7), the pendular dynamic climbing model, which is constrained to the transverse plane, was able to demonstrate the same maneuverability simply by regulating the attachment windows. This suggests the mechanisms for enabling these dynamics are within the climbing plane.

With a platform with more actuated DOFs, the attachment windows could be regulated agnostic of the out of plane dynamics. Downward climbing could be achieved by simply enforcing phase shifted attachment windows (attachment occurring near the bottom of the stroke), while strafing could be achieved by simply inducing an asymmetry in the attachment windows.

B. Identification of Gaits in Downward Climbing

In addition to identifying maneuverability within the planar dynamic model, the ground reaction force profiles from both simulation and experimentation suggest two of the previously identified the gaits in upward climbing still exist. Some of the previously identified implications of these gaits,

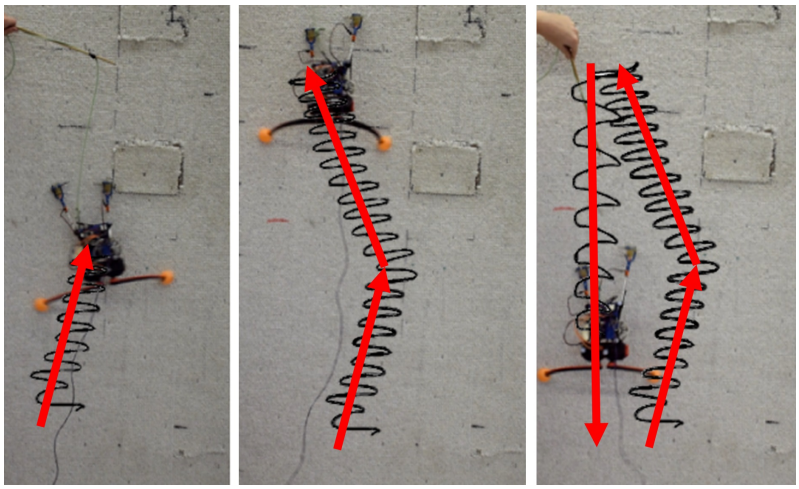

Fig. 7: A demonstration of dynamic maneuverability with TAILS, initially strafing to the right, then strafing the the left and finally a downward climbing segment.

such as walking having the lowest peak ground reaction force (which should improve attachment safety), are also maintained.

While both downward running and walking gaits appeared in simulation, only downward dynamic walking gaits were able to be achieved by TAILS. Because of the under actuated nature of TAILS, it has limited mechanisms to enable recovery from an attachment failure, which when achieved while running would result in complete detachment from the wall. It is likely that with additional leg DOFs, the downward running gaits could be experimentally achieved.

The walking and flight running gaits were identified within downward climbing, but the compliant running gaits, which are likely more secure than comparable flight running gaits, were not seen within the simulation. Since downward climbing is moving with the gravity potential field instead of against it, the gaits inherently have more energy than the upward climbing gaits, which is why at low frequencies, the downward climbing velocities are more than 3 times the upward climbing gaits. With independent of control of the attachment windows, it is possible these compliant running gaits could be generated.

C. Regulation of Out of Plane Dynamics

Even though the planar model was able to demonstrate downward climbing without directly considering the out of plane dynamics, the experimental setup required precise tuning of these body rotation dynamics to achieve fast consistent downward climbing. Within the parameter sweep, too much roll energy in upward climbing resulted in attachment failures, while downward climbing required more roll energy to enforce the attachment windows.

The impact of modifying the out of plane dynamics with the prescribed body roll is not captured by planar or quasi-static models used in this study. This suggests that to understand the interplay of these dynamics with attachment, stability, and climbing performance requires a complete 3D model.

VII. Conclusion and Future Work

In this paper, continuous dynamic maneuverability was demonstrated in both simulation and on a new climbing robot, TAILS. In the planar simulation, by defining attachment windows based on a prescribed out of plane body roll function, the model was able to achieve downward climbing.

By examining the ground reaction force profiles at low, medium, and high actuation frequencies, dynamic downward gaits were identified. The walking style gaits demonstrated the characteristic double peak ground reaction force profile, while the running style gaits at higher frequencies had single peak profiles. Experimentally, the double peak ground reaction force profile was achieved, but the current robot design could not achieve dynamic downward running.

The fact that the out of plane dynamics (not captured by the planar model) impacted the experimental platform's ability to achieve downward running gaits suggests that understanding gained from a reduced order 3D model could enable more impressive performance. Additionally, while the attachment windows were experimentally achieved using body roll, the development of a platform with additional actuated DOF could achieve these without directly influencing the out of plane dynamics, while also potentially prescribing the compliant running gait which has been shown to be beneficial to upward climbing.

Acknowledgments

The authors would like to thank Charles Young for his work developing the light weight feet. This work was supported by the collaborative participation in the Robotics Consortium sponsored by the U.S. Army Research Laboratory under the Collaborative Technology Alliance Program, Cooperative Agreement DAAD 19-01-2-0012, and by NSF Grant CMMI-1351524. The U.S. Government is authorized to reproduce and distribute reprints for Government purposes not withstanding any copyright notation thereon.

REFERENCES

[1] T. G. Miller, T. W. Bretl, and S. Rock, "Control of a climbing robot using real-time convex optimization," *IFAC Proceedings Volumes*, vol. 39, no. 16, pp. 409–414, 2006.

[2] Y. Li, A. Ahmed, D. Sameoto, and C. Menon, "Abigaille ii: toward the development of a spider-inspired climbing robot," *Robotica*, vol. 30, no. 1, pp. 79–89, 2012.

[3] S. Collins, A. Ruina, R. Tedrake, and M. Wisse, "Efficient bipedal robots based on passive-dynamic walkers," *Science*, vol. 307, no. 5712, pp. 1082–1085, 2005.

[4] P. M. Wensing and D. E. Orin, "3d-slip steering for high-speed humanoid turns," in *Intelligent Robots and Systems (IROS 2014), 2014 IEEE/RSJ International Conference on*. IEEE, 2014, pp. 4008–4013.

[5] J. Schmitt, M. Garcia, R. Razo, P. Holmes, and R. J. Full, "Dynamics and stability of legged locomotion in the horizontal plane: a test case using insects," *Biological cybernetics*, vol. 86, no. 5, pp. 343–353, 2002.

[6] A. J. McClung, M. R. Cutkosky, and J. G. Cham, "Rapid maneuvering of a biologically inspired hexapedal robot," in *ASME 2004 International Mechanical Engineering Congress and Exposition*. American Society of Mechanical Engineers, 2004, pp. 1195–1202.

[7] U. Saranli, M. Buehler, and D. E. Koditschek, "Rhex: A simple and highly mobile hexapod robot," *The International Journal of Robotics Research*, vol. 20, no. 7, pp. 616–631, 2001.

[8] M. Raibert, *Legged Robots that Balance*, ser. Artificial Intelligence. MIT Press, 1986. [Online]. Available: https://books.google.com/books?id=EXRiBnQ37RwC

[9] D. I. Goldman, T. S. Chen, D. M. Dudek, and R. J. Full, "Dynamics of rapid vertical climbing in cockroaches reveals a template," *Journal of Experimental Biology*, vol. 209, no. 15, pp. 2990–3000, 2006.

[10] G. A. Lynch, J. E. Clark, P.-C. Lin, and D. E. Koditschek, "A bioinspired dynamical vertical climbing robot," *The International Journal of Robotics Research*, vol. 31, pp. 974–996, Apr. 2012.

[11] B. D. Miller, P. R. Rivera, J. D. Dickson, and J. E. Clark, "Running up a wall: the role and challenges of dynamic climbing in enhancing multi-modal legged systems," *Bioinspiration & Biomimetics*, vol. 10, no. 2, p. 025005, 2015. [Online]. Available: http://stacks.iop.org/1748-3190/10/i=2/a=025005

[12] J. D. Dickson, J. Patel, and J. E. Clark, "Towards maneuverability in plane with a dynamic climbing platform," in *Robotics and Automation (ICRA), 2013 IEEE International Conference on*. IEEE, 2013, pp. 1355–1361.

[13] J. M. Brown, B. D. Miller, and J. E. Clark, "Classification of dynamical vertical climbing gaits," in *Intelligent Robots and Systems (IROS), 2016 IEEE/RSJ International Conference on*. IEEE, 2016, pp. 4816–4822.

[14] J. Brown, M. Austin, B. Miller, and J. Clark, "Evidence for multiple dynamic climbing gait families," *Bioinspiration & Biomimetics*, vol. Under Review, 2018.

[15] S. Kim, A. T. Asbeck, M. R. Cutkosky, and W. R. Provancher, "Spinybotii: climbing hard walls with compliant microspines," in *Advanced Robotics, 2005. ICAR'05. Proceedings., 12th International Conference on*. IEEE, 2005, pp. 601–606.

[16] J. D. Weingarten, G. A. Lopes, M. Buehler, R. E. Groff, and D. E. Koditschek, "Automated gait adaptation for legged robots," in *Robotics and Automation, 2004. Proceedings. ICRA'04. 2004 IEEE International Conference on*, vol. 3. IEEE, 2004, pp. 2153–2158.

[17] M. Austin, J. M. Brown, K. Geidel, W. Wang, and J. E. Clark, "Gait design and optimization for efficient running of a direct-drive quadrupedal robot," in *SPIE Defense+ Security*, 2017.